PHYSICAL REVIEW B VOLUME 35, NUMBER 1 1 JANUARY 1987

X-ray study of the order-disorder phase transition in the triiodide chain compound tetraphenyldithiapyranylidene iodide [DIPSΦ_4(I_3)$_{0.76}$]

P. A. Albouy and J. P. Pouget

Laboratoire de Physique des Solides, Bâtiment 510, and Laboratoire pour l'Utilisation du Rayonnement Electromagnétique, Bâtiment 209 C, Université Paris Sud, 91405 Orsay, France

H. Strzelecka

Laboratoire de Chimie et Electrochimie des Matériaux Moléculaires,
Ecole Supérieure de Physique et Chimie Industrielles de Paris, 10 rue Vauquelin, 75005 Paris, France

(Received 16 June 1986)

Tetraphenyldithiapyranylidene iodide [DIPSΦ_4(I_3)$_{0.76}$] is a one-dimensional (1D) conductor in which an organic matrix separates parallel channels filled with triiodide I_3^- anions. At room temperature, the triiodide chains present an important structural disorder characterized by the absence of long-range order along the channels and of lateral correlations between the different chains. A model of a one-dimensional harmonic liquid has been successfully used to account for the observed x-ray scattered intensity. As the temperature is lowered, coupling between the chains develops, leading to a 3D ordered state below $T_c = 182$ K. The ordering process has been studied with respect to temperature by x-ray techniques and the low-temperature structure of the iodine sublattice determined. The order which establishes below T_c is described by the Fourier components of the ionic density along a channel. They form the order parameters of the system. The temperature dependence of the first five components has been measured. They exhibit different temperature behaviors, showing the unusual character of this structural phase transition. The existing theory accounts only qualitatively for these results. The structural evolution has been correlated with the electrical properties of the material which has a Peierls-like phase transition around T_c. Starting from the fact that the first Fourier component of the iodine density corresponds to the $2k_F$ wave vector of the organic stack, a new explanation of the phase transition is proposed.

I. INTRODUCTION

A large class of organic conductors has been synthesized by the oxidation of organic donors by various halogens.[1] When iodine is used as an oxidizing agent, it generally leads to compounds containing the triiodide anion I_3^-.[1] In some of them [$TTT_2I_{3+\delta}$ (TTT is tetrathiotetracene), $B_2PI_{1.6}$ (B_2P is 5,10-dibenzylphenazinium), and $E_2PI_{1.6}$ (E_2P is 5,10-diethylphenazinium)], x-ray scattering reveals an important structural disorder of the triiodide anions in the organic matrix.[2-6] The compound $TTT_2I_{3+\delta}$ is a remarkable conductor at room temperature ($\sigma = 1000\ \Omega^{-1}\,\text{cm}^{-1}$) which undergoes a sharp metal-insulator phase transition at a temperature which depends upon its exact stoichiometry.[4] $B_2PI_{1.6}$ and $E_2PI_{1.6}$ are semiconductors.[7] The compound we study DIPSΦ_4(I_3)$_{0.76}$ (DIPSΦ_4 is tetraphenyldithiapyranylidene) has an intermediate behavior, exhibiting a broad conductor-semiconductor transition characterized by a broad maximum of conductivity around 220 K and a weak anomaly in its temperature dependence at about 165 K. This last point suggests the occurrence of a phase transition.[8,9] Such a possibility is corroborated by the observation of a well-defined angular point in the temperature dependence of the EPR linewidth[10] and an anomaly in the thermoelectric power at 165 K.[9]

Crystallographic data relevant to DIPSΦ_4(I_3)$_{0.76}$ are summarized in Table I and a projection of the structure along the stacking axis c is shown in Fig. 1.[11,12]

DIPSΦ_4 molecules are stacked along the c axis in an eclipsed manner. Two DIPSΦ_4 columns delimit a channel parallel to them. These channels are filled by triiodide anions oriented parallel to the channel direction. Raman scattering confirms I_3^- as the only species present.[12] This structure is very similar to the one of $TTT_2I_{3+\delta}$, $B_2PI_{1.6}$, and $E_2PI_{1.6}$.[4,5,7] Furthermore, the similarity of the x-ray patterns obtained with these compounds indicates that closely related structural disorders are encountered in DIPSΦ_4(I_3)$_{0.76}$.[12,13]

These structural disorders are similar to that shown by the mercury chain compounds $Hg_{3-\delta}AsF_6$.[14] This compound has a structure similar to that of a polyiodide organic conductor with the difference that the AsF_6 matrix delimits two sets of perpendicular channels filled by mercury atoms.[15] The structural disorder and the low-temperature phase transition due to the coupling between

TABLE I. Crystallographic data.

Formula	$C_{34}H_{24}I_{2.28}S_2$
Crystal system	Tetragonal
Space group	$P\bar{4}b2$
Unit cell a	19.74 Å
c	3.714 Å

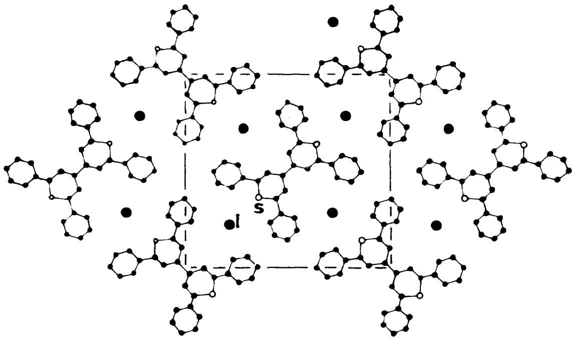

FIG. 1. (001) projection of the DIPS$\Phi_4(I_3)_{0.76}$ structure. Heavy dots point to the position of the triiodide chains in the channels.

the mercury chains have been extensively studied.[14] The in-chain disorder due to one-dimensional (1D) liquid fluctuations, has been relatively well understood[16,17] and checked experimentally. However, the theoretical predictions concerning the 1D-liquid—3D-solid phase transition have not been verified satisfactorily, probably because of competing interactions between the two interpenetrating mercury sublattices.

The purpose of this paper is to study this kind of order-disorder phase transition in a compound which possesses only one type of chain array and additionally to check the influence of the triiodide sublattice ordering on the electronic properties of the metallic organic stack. This paper has been divided as follows. Experimental techniques are briefly described in Sec. II. Characterization of the samples by their electrical properties is the object of Sec. III. In Sec. IV, the triiodide structural disorder at room temperature is analyzed and its temperature dependence studied in Sec. V. The low-temperature order-disorder phase transition is described in Sec. VI. Finally, a conclusion is drawn in Sec. VII.

II. EXPERIMENT

The molecule DIPSΦ_4 is accessible by one-step synthesis from diphyenyl-2,6-thiopyrylium salt.[8c] Small green needlelike crystals of DIPS$\Phi_4(I_3)_{0.76}$ are grown by slow evaporation of a DIPSΦ_4-iodine solution in dichloromethane with molecular ratio $m=[I_2]/[\text{DIPS}\Phi_4]<0.6$. A different stoichiometry is obtained with m larger than 0.8.[8(b),8(c)]

dc resistivity measurements between room temperature and 80 K were performed with the standard four-probes method. Contacts were made using platinum paint on parts of the crystal previously gilded by evaporation.

A first survey of the disorder and of its temperature dependence was obtained with the fixed-film—fixed-crystal method using the synchrotron x-ray beam of the station D16 of the Laboratoire pour l'Utilisation du Rayonnement Electromagnétique (LURE) at wavelengths of 1.06 and 1.58 Å. It permitted short exposure time (half an hour) combined with a high resolution [half width at half maximum (HWHM): 0.0065 Å^{-1} at 1.06 Å and 0.008 Å^{-1} at 1.58 Å using the convention $\mathbf{c}\cdot\mathbf{c}^*=2\pi$].

The quantitative measurement of the temperature dependence of Bragg spots or diffuse features has been performed with a position-sensitive detector developed in the laboratory.[18] It appeared to be especially suitable for the measurements of small features growing on a sizable background. Collections of Bragg-spot intensities for the low-temperature structural refinement (13 K) were performed with a homemade low-temperature Weissenberg camera and a three-circle goniometer (normal-beam geometry-lifting detector).

All these apparatus were equipped with a helium closed-circuit cryocooler. A minimum temperature of 10 K could be reached. They were mounted on conventional x-ray generators using the Cu $K\alpha$ radiation from (002) reflection on a doubly curved pyrolytic graphite monochromator. Photograph readings were performed with a Joyce-Loeble microdensitometer.

III. CONDUCTIVITY MEASUREMENTS

Conductivity measurements have been performed down to about 40 K by Isett *et al.*[9] and by Strzelecka and Rivory.[8(a),8(b)] The conductivity σ increases from room temperature (RT) to a flat maximum at 220 K. The ratio $\sigma_{\max}/\sigma$ (RT) is about 1.13 for both measurements. Reference 9 gives a σ (RT) of 120 $\Omega^{-1}\text{cm}^{-1}$ and Refs. 8(a) and 8(b) σ (RT)=250 $\Omega^{-1}\text{cm}^{-1}$. Below 220 K, the conductivity displays a semiconducting behavior. The effective activation energy $d\ln(\sigma)/d(1/T)$ has a small anomaly centered at 165 K and a low-temperature value of 60 meV.[9]

In order to correctly characterize our crystals, we performed conductivity measurements on three samples. Furthermore, this characterization appeared very helpful for the understanding of the low-temperature structural properties.

The behavior of the conductivity is shown by Fig. 2(a). Its temperature dependence is in agreement with that already reported in Refs. 8(a), 8(b), and 9. We have found a room-temperature conductivity of 250 $\Omega^{-1}\text{cm}^{-1}$ in agreement with the determination of Refs. 8(a) and 8(b) and a ratio $\sigma_{\max}/\sigma$ (RT) of 1.13. Figure 2(a) also shows a small anomaly at about 160 K in the temperature dependence of σ which has already been noticed in Ref. 9. It is best shown on the plot of $\Delta_{\text{eff}}=d\ln(\sigma)/d(1/T)$ [Fig. 2(b)]. We see that Δ_{eff} develops below 190 K, saturates between 170 and 150 K and then increases until about 90 K where it seems to saturate at a value close to 50 meV.

The quantity Δ_{eff} certainly deviates from the true electrical gap Δ because σ also depends upon the temperature through the carrier mobility and the temperature dependence of Δ itself (for instance, in the vicinity of a conventional Peierls second-order transition temperature, the vanishing of Δ with an infinite slope gives a divergence of Δ_{eff}).

However, in our case, as the temperature dependence of Δ_{eff} appears to be smooth, we think that, at least qualitatively, it mimics the behavior of the electrical gap Δ on the DIPSΦ_4 chains. This behavior will be discussed in Sec. VI in connection with structural quantities measured on the iodine sublattice.

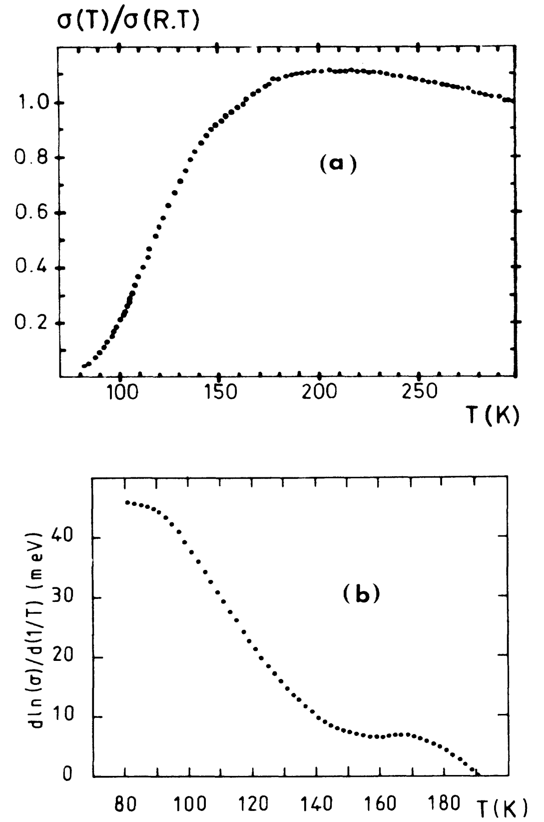

FIG. 2. (a) Temperature dependence of the normalized dc conductivity of $DISP\Phi_4(I_3)_{0.76}$. Experimental points are an average of the data obtained with three samples. (b) Temperature dependence of the effective activation energy $\Delta_{eff} = d\ln(\sigma)/d(1/T)$.

IV. ANALYSIS OF THE DISORDER AT ROOM TEMPERATURE

A. Experimental data

The x-ray pattern of Fig. 3 reveals two different features. First, it shows well-defined Bragg-spot layers perpendicular to the *c* axis which correspond to the diffraction by the organic matrix. Their spacing gives the *c* parameter of the crystal, $c = 3.714$ Å. Second, one can see intense diffuse lines, also perpendicular to the *c* axis. These lines have been observed whatever the orientation of the crystal around the *c* axis. They are thus coming from the intersection of the Ewald sphere with diffuse sheets perpendicular to the *c* axis in the reciprocal space. As shown on Fig. 4, the diffuse lines have an intensity distribution in the *c* direction which resembles that shown by the other triiodide compounds $TTT_2I_{3+\delta}$, $B_2PI_{1.6}$, and $E_2PI_{1.6}$.[2,3]

It is possible to distinguish two sets of diffuse lines on the photograph of Fig. 3. The first family contains what we have called main lines, labeled by an index *l* running from one to ten on Fig. 3. These lines are equally spaced and their width increases rapidly with increasing line index *l*. As the resolution remains practically constant in such a geometry, the broadening is an intrinsic phenomenon. Furthermore, one can notice that the intensity of the first three main lines is slightly modulated. The additional lines which form the second family are shown by arrows on Fig. 3.

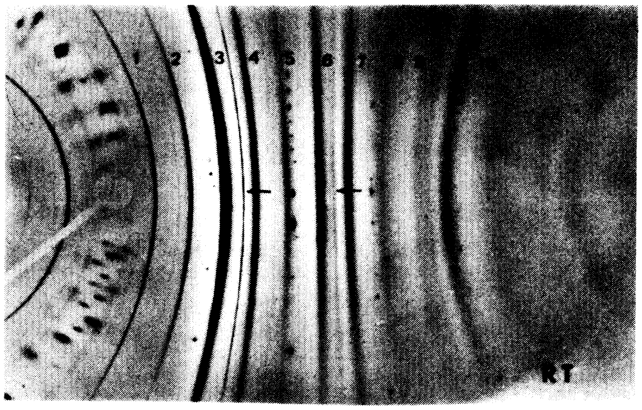

FIG. 3. Fixed-film fixed-crystal x-ray pattern of the $DIPS\Phi_4(I_3)_{0.76}$ single crystal taken at station D16 of LURE at room temperature ($\lambda = 1.06$ Å). The *c* axis is horizontal, *l* indices are for main lines, arrows for additional lines.

B. Qualitative discussion of the main lines

Structural refinements of $DIPS\Phi_4(I_3)_{0.76}$ crystals have shown that the positions of the atoms of the $DIPS\Phi_4$ matrix can be easily determined from the Bragg-spot intensity analysis.[11,12] On the other hand, the iodine contribution deduced is highly deficient and an enormous thermal agitation of the iodine atoms along the *c* axis is found. Thus it is tempting to attribute the diffuse intensity mainly to the triiodide chains. A more direct evidence is that a contribution of the $DIPS\Phi_4$ molecules to the diffuse intensity would strongly modulate the intensity of each line through the molecular structure factor of $DIPS\Phi_4$. The triiodide anions which are parallel to the *c* axis do not have this effect. Actually, the intensity of the diffuse lines is uniform except for the first three main lines, which show a slight periodic modulation, each having a different origin. Finally, the clearest evidence is the sharp increase of the intensity of the main lines of index 3, 4, 6, and 7 shown by Fig. 3 and which is due to the molecular structure factor of the triiodide anions. This feature, already discussed in Ref. 3 for $B_2PI_{1.6}$ and $E_2PI_{1.6}$ will be quantitatively discussed in part C of this section.

The distribution of the diffuse intensity in sheets is explained if there is no phase coherence between the triiodide chains. The slight intensity modulation of the first lines indicates only a very short-range order between neighboring chains. This will be discussed in Sec. V B. In a first approximation, we shall neglect this coupling and consider each chain as independent of the others. In the following, we shall discuss the main lines. Additional lines will be the object of part D of this section.

If one considers an infinite linear chain of spacing *d*, the corresponding reciprocal lattice consists of infinitely

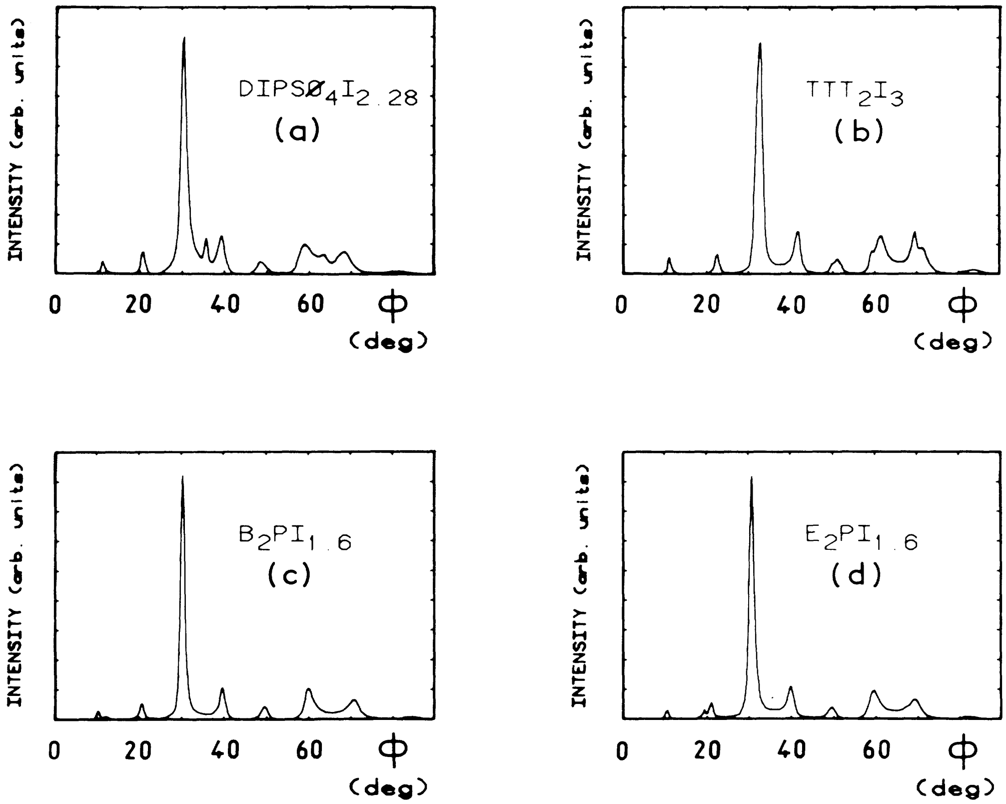

FIG. 4. Microdensitometer readings of x-ray patterns from four triiodide chains compounds is a direction perpendicular to the diffuse lines: (a) $\mathrm{DIPS\Phi_4(I_3)_{0.76}}$, (b) $\mathrm{TTT_2I_{3+\delta}}$, (c) $\mathrm{B_2PI_{1.6}}$, (d) $\mathrm{E_2PI_{1.6}}$. The orientation is the same for all the crystals (Φ signifies the scanning angle of the x-ray pattern).

sharp sheets perpendicular to the chain direction spaced by $2\pi/d$.[19] In experimental conditions, these sheets have the same width as that given by the resolution. This is well observed in partly polymerized diacetylene crystals, for instance.[20] If the position of the units is disturbed in such a way that the fluctuations of distance are independent of the distance between the units, then long-range order is kept, the sharpness of the sheets is conserved, but their intensity is changed (first-kind disorder). For instance, in the case of thermal agitation around a fixed position, the reduction of intensity is described by the introduction of a Debye-Waller factor. In our case, the rapid increase of the linewidth can be explained only if one admits that there is no long-range order along the chains, i.e., the existence of cumulative fluctuations of distance (second-kind disorder).[19] Similar features are observed in the compounds $\mathrm{Hg_{3-\delta}AsF_6}$ [Refs. 14(c)–14(e)], $\mathrm{E_2PI_{1.6}}$ and $\mathrm{B_2PI_{1.6}}$ (Refs. 3 and 6), and $\mathrm{TTT_2I_{3+\delta}}$[2,5] (see Fig. 4). They can be interpreted in models of 1D positional disorder of a given species which are detailed in part C of this section. A different explanation involving a complex statistical distribution of $\mathrm{I_2}$ and $\mathrm{I^-}$ species in chains of $\mathrm{I_3^-}$ species has been proposed in Ref. 5 for $\mathrm{TTT_2I_{3+\delta}}$. This possibility will be ruled out for $\mathrm{DIPS\Phi_4(I_3)_{0.76}}$ in part C of this section.

The repeat distance between main lines leads to a periodicity $d = 9.79$ Å. It represents the average distance between triiodide units in a chain and this value is in good agreement with previous reports on similar triiodide compounds.[21] This periodicity d is incommensurate with the periodicity c of the host lattice. With two iodide chains per $\mathrm{DIPS\Phi_4}$ chain, the ratio d/c leads to a $[\mathrm{I_3}]/[\mathrm{DIPS\Phi_4}]$ structural stoichiometry of 0.76, in good agreement with the chemical stoichiometry of our samples.[8(b)] With a charge transfer of one electron per $\mathrm{I_3^-}$ unit, the periodicity d is identical to the wavelength associated to the $2k_F$ wave vector of the 1D electronic gas on the $\mathrm{DIPS\Phi_4}$ chains, $d = 2\pi/2k_F$. This has some important consequences on the electronic properties of the material (see Sec. VI B 1).

C. Model of disorder in chain direction

A model of 1D liquid fluctuations has been proposed by Emery and Axe to account for the properties of the compound $\mathrm{Hg_{3-\delta}AsF_6}$.[16] The chains are treated as independent and the intrachain interactions are supposed harmonic and between first neighbors. In this model, the disorder is dynamic in nature. It has been developed in detail by Yoshida *et al.*[17] A slightly different approach has been used by Endres *et al.*[3] and Rosshirt *et al.*[6] for the compounds $\mathrm{B_2PI_{1.6}}$ and $\mathrm{E_2PI_{1.6}}$. Starting from the fact that x-ray diffraction does not give information on the dynamics of the fluctuations, they used the description of the paracrystal.[19] A distribution function of the first neighbors $h_1(z)$ is introduced where z is the deviation to the average distance d between I_3^- units. The parameters of this function are adjusted to fit the experimental data. In the case of a Gaussian distribution

$$h_1(z)=\exp(-z^2/2\sigma^2)\ , \tag{1}$$

the structure factor $S^0(q_z)$ is identical to that obtained with a model of 1D-harmonic liquid:

$$S^0(q_z)=\frac{\sinh(q_z^2\sigma^2/2)}{\cosh(q_z^2\sigma^2/2)-\cos(q_z d)}\ , \tag{2}$$

where q_z is the c axis component of the scattering vector **q**. In the 1D-harmonic liquid theory, the mean-square fluctuation between first neighbors σ^2 is related to the temperature, the mass of the molecules m and the sound velocity in the chain direction v by

$$\sigma^2=\frac{k_B T}{mv^2}d^2\ . \tag{3}$$

Additional parameters can be added in the function $h_1(z)$ (Ref. 6) or, equivalently, anharmonicity can be added to the harmonic interaction potential.[14(e)] In a first step, we started from Eq. (2) keeping the harmonic approximation. We suppose also that the triiodide units are linear and symmetric, naming δ the distance between two adjacent iodine atoms of an I_3^- unit. As in Ref. 3, no Debye-Waller factor was introduced to account for the internal motions of the I_3^- molecules.

The new intrachain structure factor is given by

$$\begin{aligned} S'^0(q_z) &= \langle \rho_I(q_z)\rho_I(-q_z)\rangle \\ &= [1+2\cos(q_z\delta)]^2 S^0(q_z)\ , \end{aligned} \tag{4}$$

where $\rho_I(q_z)$ is the Fourier transform of the iodine density in the chain direction and $1+2\cos(q_z\delta)$ the geometrical structure factor of a I_3^- unit. The intensity scattered by a chain can be put under the form

$$I(\mathbf{q})=|f_I(\mathbf{q})|^2 S'^0(q_z) \tag{5}$$

where $f_I(\mathbf{q})$ is the atomic x-ray scattering factor of iodine.

We see on Figs. 5(a) and 5(b) that the experimental intensity distribution is well accounted for by the theoretical expression (5) with the two parameters $\sigma=0.35$ Å and $\delta=3.00$ Å. This last value is in good agreement with I-I distances of I_3^- units reported in the literature.[21] The value of σ is very similar to that found in $E_2PI_{1.6}$ and $B_2PI_{1.6}$ at room temperature, $\sigma=0.30$ Å.[3] Within the experimental accuracy of our data, no extra parameter is necessary. The small value of σ/d (0.035) means that the fluctuations are correlated over a long distance. In this limit, for $q_z\sigma<1$, $S^0(q_z)$ can be decomposed under a sum of well-separated Lorentzian peaks, each centered at $q_z=\pm 2\pi l/d$ where l is an integer. Their half width at half maximum (HWHM) Δl is related to σ by the relationship[16,17]

$$\Delta l = 2\pi^2 l^2\sigma^2/d^3\ \text{Å}^{-1}\ . \tag{6}$$

This law has been previously checked in $Hg_{3-\delta}AsF_6$,[14(d),14(e)] $B_2PI_{1.6}$ and $E_2PI_{1.6}$,[3] and is well verified for $DIPS\Phi_4(I_3)_{0.76}$ (see also Sec. V A).

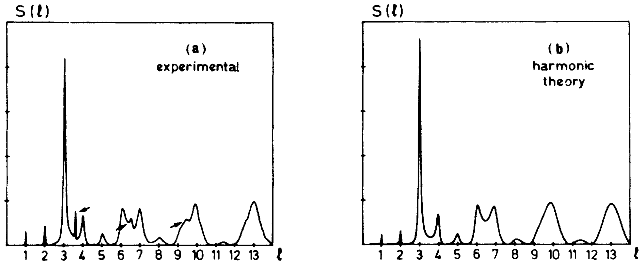

FIG. 5. (a) Microdensitometer reading of the diffuse intensity along the c direction of the x-ray pattern of Fig. 3. The intensity has been corrected for absorption, polarization, and iodine atomic scattering factor. The abscissa l is given in d^* unit. Arrows point to the additional lines. (b) Convolution of the theoretical intensity $S^0(q_z)$ given by (4) with the experimental synchrotron resolution (HWHM of 0.0065 Å^{-1}). The values of the adjustable parameters are $\sigma=0.35$ Å and $\delta=3.00$ Å.

A different explanation of the broadening of the diffuse lines has been proposed for the compound $TTT_2I_{3+\delta}$ in Ref. 5. It supposes that I_2 and I^- species are intercalated between I_3^- units, leading to a static disorder. Besides the fact that I_2 species have not been observed by Raman scattering in $DIPS\Phi_4(I_3)_{0.76}$,[12] such an organization would prevent the establishment of long-range order between the iodine chains, in contradiction with our experimental findings (see Sec. V).

D. Additional satellite lines

The positions of the additional lines observed on Fig. 3 have been listed in Table II. It is easy to check with these values that all the positions can be written as a main line index plus or minus about 2.64. The reciprocal parameter c^* of the organic matrix, expressed in d^* units, is $\tilde{c}=d/c=2.64$. Thus, each additional line can be related to a main line by the addition or subtraction of $\tilde{c}$. Furthermore, one can verify that the more intense lines of index $l=3.64$ and $l=6.62$ have the same width as the main line they are related to (lines of indices 1 and 4, respectively). The family of additional lines can be thus explained by a modulation of the triiodide chains by the host lattice.[13] It is not necessary to suppose the existence of a second family of chains, as it was postulated before for $TTT_2I_{3+\delta}$,[2] $E_2PI_{1.6}$, and $B_2PI_{1.6}$.[3] In our case, this additional periodicity corresponds to the first Fourier component of the external potential created by the host lattice upon the chains. This potential can be due to small bottlenecks

TABLE II. Positions of the additional lines expressed in σ^* units.

Position	Intensity
1.64	weak
3.64	strong
4.64	weak
5.68	weak
6.62	strong

created by the sulfur atoms of the DIPSΦ_4 molecules in the channels as shown by structural data (see Fig. 1). At a lower temperature, it is also possible to observe second Fourier components of this potential, that is additional lines separated from a main line by $\pm 2\tilde{c}$. The modulation of a 1D liquid by a host lattice potential has been treated in conjunction with superionic conductors problems.[22,23] Different potentials and intrachain interactions have been considered. However, because of the strongly correlated nature of the 1D liquid, our case might be described by the Frenkel-Kontorava model.[23] Unfortunately, the use of this model in Ref. 23 predicts a strong temperature dependence of the modulation which is not observed experimentally (see also Sec. VI A 3 *b*). We preferred thus to choose a simpler model where the effect of the host lattice is to produce a displacive modulation of the triiodide units by a wave of amplitude u and wave vector $c^* = 2\pi/c$.[24] As the intensity of each satellite line is uniform, the modulation is only polarized in chain direction. It leads to a new structure factor,

$$S'^0(q_z) + \left[\frac{q_z u}{2} \right]^2 S'^0 \left[q_z \pm \frac{2\pi}{c} \right] . \tag{7}$$

This expression shows clearly that the main lines and their satellite lines have the same width. By adjustment on the two more intense satellite lines, one gets $u = 0.13$ Å. The modulation is in fact weak, the strong intensity of some additional lines being the effect of the molecular structure factor of I_3^- units. Additional lines observed on the compounds $TTT_2I_{3+\delta}$, $E_2PI_{1.6}$ and $B_2PI_{1.6}$ can be explained in a similar manner.

The displacive modulation of the triiodide chains by the host lattice could also explain some of the difficulties encountered in the structural refinements. In the absence of modulation, the contribution of the iodine atoms to the Bragg scattering should be restrained to the ($hk0$) plane. In other terms, the iodine density along the channels would be constant. Its Fourier transform should thus present a unique Bragg-like peak at $q_z = 0$. A contamination of higher-l Bragg reflections by the 1D diffuse scattering of the chains is possible but should be removed by the background correction. The authors of Refs. 11 and 12 have found a coherent contribution of iodine in planes of higher-l index. To account for this fact, a percentage of commensurability of iodine has been introduced in Ref. 11. Although the refinement procedure appears successful, they get a Debye-Waller factor of the iodine atoms which diverges.[11] This can be explained by the displacive modulation of the triiodide chains. By this effect, the iodine density presents a permanent modulation (inhomogeneous liquid). Its Fourier transform has thus additional peaks at $q_z = \pm 2\pi n/c$ where n is an integer.[22] This very particular contribution to the Bragg scattering cannot be traduced by a mere Debye-Waller factor.

V. TEMPERATURE BEHAVIOR

We shall describe here the effect of the temperature on the parameters which describe the intrachain disorder and the short-range lateral correlations.

A. Intrachain disorder

We have seen in Sec. IV that the fluctuations of an I_3^- unit around its average position are described by the parameter σ related to the temperature by the relation (3), $\sigma^2 = (k_B T / m v^2) d^2$. The HWHM of the lth lines is related to σ^2 in Eq. (6): $\Delta l = 2\pi^2 l^2 \sigma^2 / d^3$. The parameters σ^2 deduced from the HWHM of main lines 4 and 7 have been plotted on Fig. 6 as a function of temperature. It shows that both determinations give the same value of σ and thus that relation (6) is kept throughout the temperature range. Furthermore, σ^2 decreases linearly with temperature as predicted by (3). σ can be extrapolated at zero for $T = 0$ K. Relation (3) leads to a sound velocity of 2290 ms^{-1} at room temperature in the channel direction. Measures down to 120 K on the mercury chain compound have shown a similar behavior of the σ parameter.[14(a)] In $E_2PI_{1.6}$, σ saturates at about 100 K, perhaps because of the quenching of the disorder.[3]

B. Interchain correlations

1. Experimental data

At room temperature, very weak modulations of the first three main lines are observed (see Fig. 3). It reflects the existence of weak lateral interchain correlations which have been neglected in the analysis performed in Sec. IV. The x-ray pattern shown in Fig. 7 exhibits a noticeable reinforcement of the modulations of the first main line at 200 K. It reflects the increase of the interchain coupling on cooling down. It can be noticed that the same phenomenon appears on its first harmonic of modulation

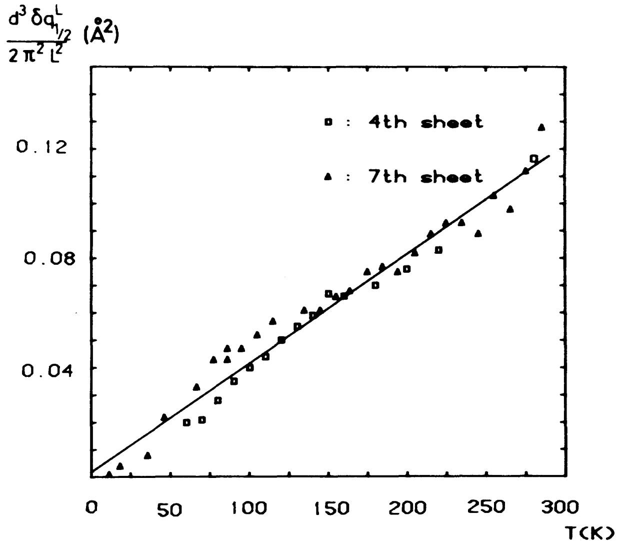

FIG. 6. Temperature plot of the square of the parameter σ. Determination from the main lines $l = 4$ has been made on high-resolution photographs taken at LURE (resolution: HWHM of 0.008 Å^{-1}). Determination from main lines $l = 7$ has been made with a position sensitive detector (resolution: HWHM of 0.010 Å^{-1}). The straight line is a least square fit. The small intercept at $T = 0$ K is not meaningful.

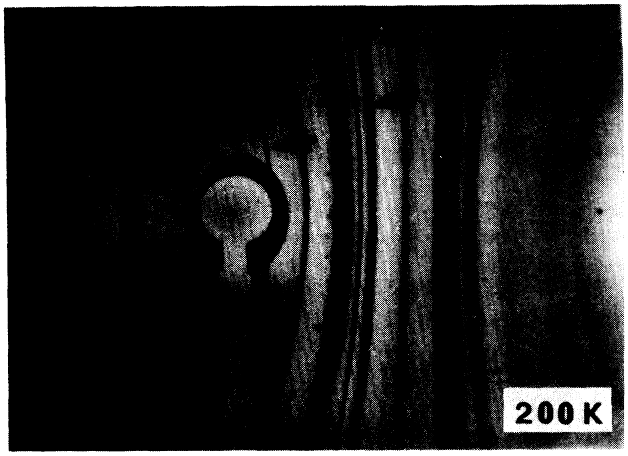

FIG. 7. Fixed-film crystal x-ray pattern of a DIPS$\Phi_4(I_3)_{0.76}$ single crystal taken at station D16 of LURE at 200 K ($\lambda = 1.58$ Å). The c axis is horizontal. Arrows point to intensity reinforcements on the first main line and its first harmonic of modulation. Right-hand arrow points to the second harmonic of modulation of the first main line.

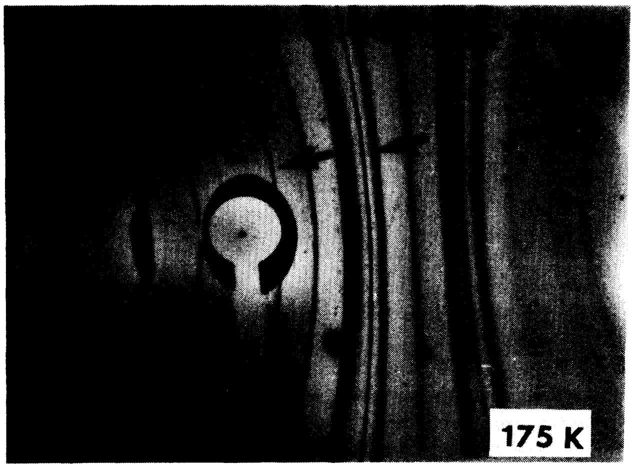

FIG. 8. X-ray pattern obtained in the same conditions as in Fig. 7 but with $T = 175$ K. Bragg reflections are visible on the first main line and its satellites of modulation.

and that a second harmonic of modulation is now visible. The x-ray pattern of Fig. 8 taken at 175 K shows that these modulations have clearly condensed into Bragg reflections on the first main line and its satellites of modulation. The long-range order is thus established. The increase of lateral correlations when T decreases is well illustrated on Fig. 9. The diffuse intensity along the first main line has been recorded with a position sensitive detector in the [110] direction. The scan obtained at 10 K has a nearly Gaussian line shape. Its HWHM of 0.010 Å^{-1} corresponds to the experimental resolution measured on a Bragg reflection of the host lattice.

The expression of the scattered intensity in a system of coupled chains will be derived in part 2 of this section.

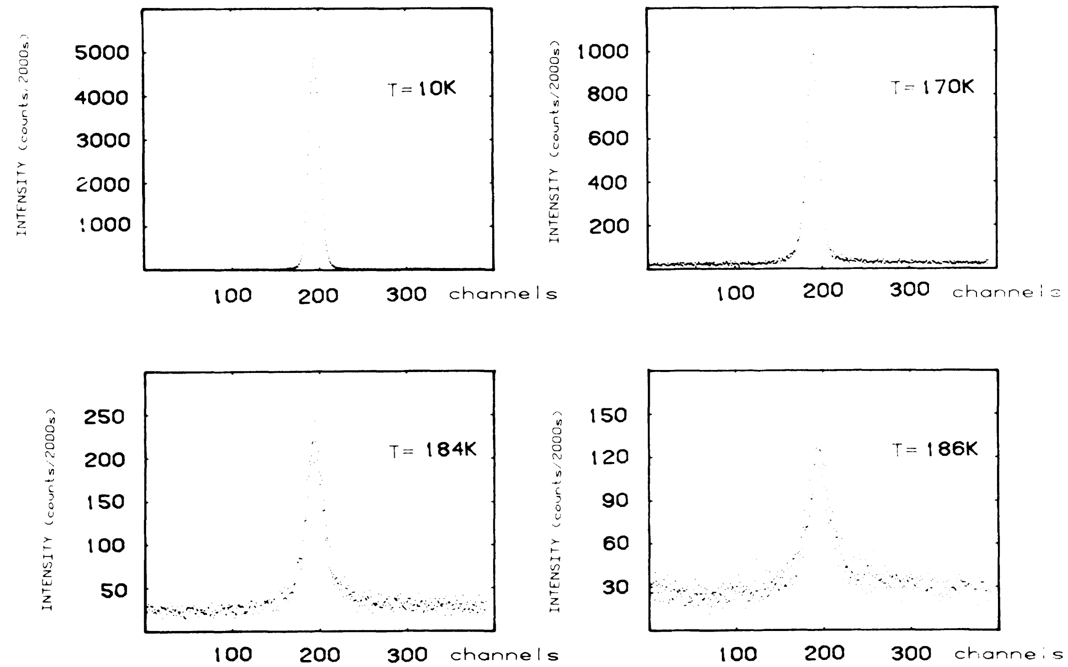

FIG. 9. Position sensitive detector scans along the first iodine main lines in the [110] direction at $T = 186$, 184, 170, and 10 K. The first two scans have been recorded above T_c and the two latter ones below T_c. The 10-K scan gives the experimental resolution (one channel $= 0.0012$ Å^{-1}).

Let us just mention here that it takes the form

$$I(\mathbf{q}) \propto S(\mathbf{q}) = k_B T \chi(\mathbf{q}) \ , \tag{8}$$

At the critical wave vector q_c for which $\chi(\mathbf{q})$ diverges, the quantity I/T measures the divergence. Figure 10(b) shows by the plot of T/I that in the vicinity of T_c, χ^{-1} follows the mean-field behavior $\chi^{-1} \propto (T-T_c)$ with a $T_c = 182$ K. In the vicinity of q_c, $\chi(\mathbf{q})$ has generally a Lorentzian shape. More explicitly for $q = q_c + \delta q$ in the [110] direction, one has

$$\chi(q) = \frac{\chi(q_c)}{1+\xi_\perp^2 \delta q^2} \ , \tag{9}$$

where $\xi_\perp$ is the correlation length in this direction. The temperature dependence of $\xi_\perp^{-1}$ deduced from the data after correction by the experimental resolution (Voigt profile correction[25]) is given by Fig. 10(a). $\xi_\perp$ varies from 18 Å at 214 K to 83 Å at 184 K. The transition temperature T_c can be deduced from a plot of this temperature variation by the mean-field result $\xi_\perp^{-1} \propto (T-T_c)^{1/2}$. The best fit leads also to a $T_c = 182$ K.

Bragg spots appear at the $(h/2, k/2, l=1)$ positions with h and k odd (see Sec. VI A 3a), using the (a^*, b^*, d^*) reciprocal plane. The modulations on main line $l=2$ are extremely weak and are not critical. Well-defined Bragg reflections appear below 175 K at positions $(h, k, l=2)$ with h and k integers.

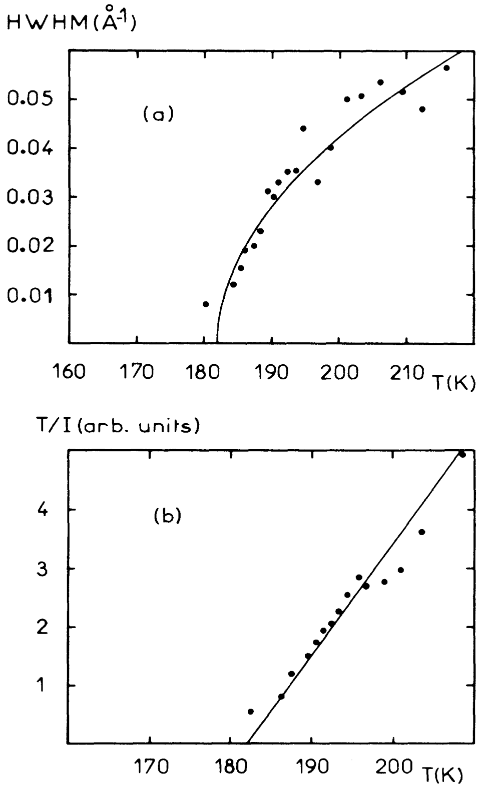

FIG. 10. (a) Half width at half maximum of the intensity modulations of the first main line versus temperature (scans of Fig. 9). A Voigt-type resolution correction has been applied. The solid curve is a best fit with the mean field formula $\xi_\perp^{-1} \propto (T-T_c)^{1/2}$ with $T_c = 182$ K. (b) Temperature plot of the inverse of the peak intensity of the modulation of the first iodine main line corrected by the thermal population factor, T/I. Solid line is a best fit by the mean-field formula $\chi^{-1} \propto (T-T_c)$ giving $T_c = 182$ K.

The high intensity of the third main line authorized us to follow the temperature dependence of its intensity modulations as shown by the diffractometric scans of Fig. 11. Surprisingly, it shows at room temperature and below broad maxima at positions which seem to be incommensurate with respect to the DIPSΦ_4 lateral (a^*, b^*) reciprocal plane. Its extreme spreading in directions perpendicular to the c axis did not allow an accurate indexation of the positions of the maxima ($q_a = q_b \simeq \pm 0.31 a^*$ on Fig. 11). The HWHM is found to be temperature independent from room temperature down to 130 K. It corresponds to a very short correlation length of about 13 Å. The amplitude of the broad modulations grows by a factor 4 from room temperature to 130 K. These features show that this incommensurate phasing of iodine chains does not behave critically when the temperature decreases. As shown on Fig. 11, Bragg reflections appear around 150 K at the positions $(h/2, k/2, l=3)$, with h and k odd, which are clearly different from that of the broad maxima, but which are identical to that shown by the first main line. Below 130 K, the broad modulations are overwhelmed by the Bragg reflections. Figure 11 shows that the Bragg spots appear without sizable pretransitional critical fluctuations on the third main line.

2. *Discussion*

These data clearly show that the phase transition undergone by the compound DIPSΦ_4(I$_3$)$_{0.76}$ cannot be classified as a conventional structural phase transition where the critical fluctuations are identical for every wave vector of the reciprocal space where satellite reflections appear below T_c. Here, only the fluctuations observed on the $l=1$ main line (and associated satellite lines) are critical at T_c. The absence of sizable critical fluctuations on diffuse sheets of high-l index was noticed before in Hg$_{3-\delta}$AsF$_6$ [Ref. 14(b)], E$_2$PI$_{1.6}$, and B$_2$PI$_{1.6}$ (Ref. 3).

Another unusual feature is the presence of two different short-range orders describing two different ways of phasing between the chains. Two competing ordering wave vectors were also observed in Hg$_{3-\delta}$AsF$_6$ [Refs. 14(a) and 14(b)]. However, in this compound, they were understood as reflecting the competition between parallel chain-chain interactions and orthogonal chain-chain interactions.[16] This is of course not the case in DIPSΦ_4(I$_3$)$_{0.76}$ for which all the chains are parallel.

These factors can be discussed in the framework of the mean-field theory developed by Emery and Axe.[16] The interactions between the triiodide chains are supposed to be Coulombic in nature. If $\rho_{\mathrm{el}}^{\alpha}(z)$ is the charge density along the αth chain, the coupling energy between the chains can be written as

$$H = -\tfrac{1}{2} \sum_{\alpha} \sum_{\beta} \int \int v_{\alpha\beta}(z-z') \rho_{\mathrm{el}}^{\alpha}(z) \rho_{\mathrm{el}}^{\beta}(z') dz dz' \ . \tag{10}$$

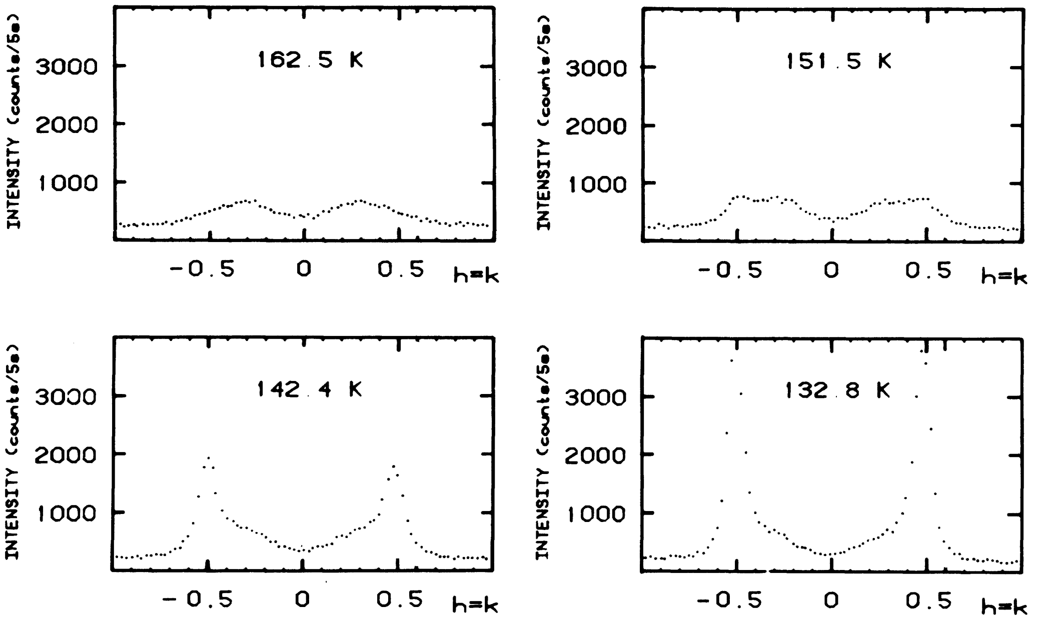

FIG. 11. Diffractometric scans along the [110] direction of the third main iodine line at $T=162.5$, 151.5, 142.4, and 132.8 K. The maxima of the high-temperature broad modulations are at h and $k \simeq \pm 0.31$. Bragg reflections appear at h and $k = \pm 0.5$ on the last three scans. One can notice the coexistence of the two kinds of modulations on these scans.

With a Fourier transform in the chain direction, it becomes

$$H=\frac{1}{2}\sum_{\alpha}\sum_{\beta}\int v_{\alpha\beta}(q_z)\rho^{\alpha}_{\mathrm{el}}(q_z)\rho^{\beta}_{\mathrm{el}}(-q_z)dq_z \ . \qquad (11)$$

At this stage it is useful to introduce the Fourier transform of the particle (I_3^- unit) density on the αth chain $\rho^{\alpha}(q_z)$, which is the quantity describing the phase transition. Thus one has simply,

$$\rho^{\alpha}_{\mathrm{el}}(q_z)=\sigma_{\mathrm{el}}(q_z)\rho^{\alpha}(q_z) \qquad (12)$$

where $\sigma_{\mathrm{el}}(q_z)$ is the Fourier transform of the charge distribution on an I_3^- unit. In the classical approximation implicitly considered in (8),

$$S(q)=\langle\rho(\mathbf{q})\rho(-\mathbf{q})\rangle=k_BT\chi(\mathbf{q}) \ . \qquad (13)$$

This quantity is related to the x-ray scattered intensity by expressions (4) and (5), where $S(q)$ replaces $S^0(q_z)$. In the mean-field approximation, $\chi(\mathbf{q})$ is given by[16]

$$\chi(\mathbf{q})=\chi^0(q_z)/[1-v(\mathbf{q})\,|\sigma_{\mathrm{el}}(\mathbf{q}_z)|^2\chi^0(q_z)] \ , \qquad (14)$$

with

$$v(\mathbf{q})=\frac{1}{N}\sum_{\alpha,\beta}v_{\alpha\beta}(q_z)e^{i\mathbf{q}\cdot\mathbf{R}_{\alpha\beta}} \ . \qquad (15)$$

(N is the number of chains, $R_{\alpha\beta}$ describes the lateral position of the chains.)

$\chi^0(q_z)$ is the intrachain response function related to $S^0(q_z)$, defined in (2) by

$$S^0(q_z)=k_BT\chi^0(q_z) \ . \qquad (16)$$

If one supposes that the ionic charge is equally distributed upon the three atoms of a triiodide unit, one has[31]

$$\sigma_{\mathrm{el}}(q_z)=\tfrac{1}{3}[1+2\cos(q_z\delta)] \ . \qquad (17)$$

The intensity scattered by the coupled iodine chains is the generalization of expression (5),

$$\mathrm{I}(\mathbf{q})=|f_{\mathrm{I}}(\mathbf{q})|^2S(\mathbf{q}) \ .$$

The new structure factor is given by

$$S(\mathbf{q})=S'^0(q_z)\Big/\left[1-\frac{v(\mathbf{q})}{9k_BT}S'^0(q_z)\right] , \qquad (18)$$

where $(S')^0(q_z)$ is the structure factor observed in absence of lateral correlations [expression (4)].

Lateral correlations are described by the wave vectors providing a minimum in the denominator of (18). Several kinds of local order can be achieved for different values of q_z (i.e., line index) because of the presence of two competing parameters in (18):

(i) The coupling energy $v(\mathbf{q})$: In the case of a Coulomb interaction (even screened by the organic sublattice) this quantity decreases with increasing q_z component.[16]

(ii) The structure factor of 1D-liquid fluctuations $S'^0(q_z)$: It presents well-defined peaks centered at $q_z=\pm 2\pi n/d$ and an important maximum for $q_z=\pm 6\pi/d$. This behavior is due to the correlated nature of the 1D liquid and to the charge distribution of an I_3^- unit (see Fig. 5).

The parameter $v(\mathbf{q})$ favors the development of a short-range order on the first diffuse line, while the parameter $S'^0(q_z)$ favors a different short-range order on the third diffuse line. The q_z variation of these two parameters is probably so contrasted that only a very slight short-range order is found on the second diffuse line. Main lines of indices $l>4$ do not present sizable short-range order, which means that the right-hand side of the denominator of (18) remains small compared to unity.

In DIPS$\Phi_4(I_3)_{0.76}$ the stabilization at T_c of the critical wave vector $\mathbf{q}_c=(h/2,k/2,l=1)$ with h and k odd means that the divergence of (18) is achieved by the coupling term $v(\mathbf{q})$. We also reinvestigated the disordered variety of $TTT_2I_{3+\delta}$ and found that at the difference of DIPS$\Phi_4(I_3)_{0.76}$, the fluctuations at $q_z=\pm 6\pi/d$ and not that at $q_z=\pm 2\pi/d$ are critical ($T_c \simeq 170$ K).[26] In $E_2PI_{1.6}$, an incommensurate short-range order is also observed at room temperature for $q_z=\pm 6\pi/d$ in the sample investigated in Ref. 3. But these fluctuations do not lead to the establishment of a long-range order at lower temperatures.[3]

VI. THE LOW-TEMPERATURE ORDERED PHASE

A. Experimental data

1. *Order parameters*

Below T_c, Bragg spots progressively appear on lines of higher index reflecting a progressive development of the various Fourier components describing the long-range order. On the x-ray pattern of Fig. 12 taken at 70 K, Bragg spots are visible on all the observable main lines. The formation of sharp Bragg reflections allow us now to see first and second harmonics of modulation of more main lines.

It is important to notice that the diffuse scattering has not disappeared below the temperature of transition. Furthermore one can see on lines of high index that their HWHM remains larger than the experimental resolution. This important diffuse scattering is observed whatever the cooling rate, thus excluding a quenching effect.

According to the theory of Ref. 16, the ordering process of a chain can be described by the Fourier components $\rho(q_z)$ of the particle (I_3^- units) density in chain direction. The average structure is accounted for by the components at $q_z=\pm 2\pi l/d$ where l is an integer. The modulation due to the host lattice is brought in by the components at $q_z=\pm 2\pi l/d \pm 2\pi n/c$ where l and n are integers. The low-temperature structure (see part 3) reveals that all the chains are described by the same $|\rho(q_z)|$ but with different phase shifts. The intensity of a Bragg reflection appearing on the lth main line is thus proportional to $|\rho(q_z=2\pi l/d)|^2$. We have plotted on Fig. 13 the temperature dependence of Bragg reflection intensity of main lines ranging from one to five. The (h,k) index of the Bragg reflections of the iodine sublattice with respect to the host lattice will be specified in part 3. $|\rho(l=1)|^2$ increases nearly linearly from T_c to 140 K. Below 130 K, it remains practically constant. The deviation from linearity around T_c is due to an important critical scattering superimposed to the Bragg reflection, which enhances slightly the peak intensity. The other components $|\rho(l)|^2$ have a smoother behavior with $|\rho(3)|^2$, $|\rho(4)|^2$, and $|\rho(5)|^2$ displaying very similar temperature dependences. The intensity of the first harmonic of modulation of the first main line (at $l \simeq 3.66$) displays the same temperature dependence as the Bragg reflections of the parent line $l=1$ (Fig. 13). This behavior is consistent with that shown by the pretransitional fluctuations.

It is interesting to correlate the temperature dependence of the lth order parameter with that of the corresponding diffuse line. For that purpose we have recorded as a function of temperature the profile of the diffuse lines midway between the Bragg spots. This is exemplified by Fig. 15 for the third and fourth diffuse lines. We have plotted in Fig. 14 the corresponding integrated intensity for the first four main lines as a function of temperature. As expected from the 1D-harmonic liquid theory, the integrated intensity remains almost constant above T_c.[17] This feature is well illustrated on Fig. 15 for the third main line; as the temperature decreases, the HWHM decreases and the peak intensity increases. Below T_c, one can notice that the intensity of a diffuse line and the intensity of the corresponding Bragg reflections have opposite behaviors. By extrapolation at $T=0$ K, we see that "1D-liquid" fluctuations do not disappear.

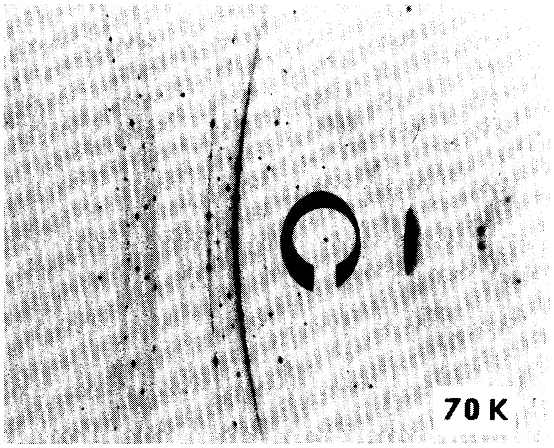

FIG. 12. X-ray pattern obtained in the same conditions as in Fig. 7 but with $T=70$ K. Bragg reflections are visible on all the diffuse lines.

2. *Lattice parameters*

The temperature dependences of the more relevant parameters of the crystal, d and c, have been determined (see Fig. 16). Parameter c was precisely determined from Bragg-reflection positions of the host lattice with the low-temperature goniometer. The room temperature value is c (300 K) = 3.716 Å in excellent agreement with previous determinations.[10,11] The low-temperature value is c(13 K) = 3.648 Å and no anomaly appears at T_c. Due to the lack of long-range order of the triiodide chains above T_c, the parameter d is much more difficult to measure precisely. It was determined on photographs from the distance between main lines $l=-3$ and $l=3$ which remain intense even at low temperature and are not too broad. The precision is rather poor, about 0.5%. The value at 13 K was precisely measured with the low-temperature goniometer from the Bragg reflections positions of the iodine sublattice, d (13 K) = 9.705 Å. At this temperature, the ratio of both parameters is:

$d/c\,|_{13\,\mathrm{K}}=2.66$. At the precision of our measurements, the two periods are thus commensurate with $d/c=8/3$. Although the precision on d is poor, it seems to remain commensurate up to around 130—140 K.

It is interesting to notice that d remains practically constant above T_c, which is consistent with an harmonic interaction between I_3^- units within a channel.

3. Structure at 13 K

The low-temperature structure of the triiodide chains sublattice has been determined by the analysis of 352-Bragg-reflection intensities collected at 13 K. The data collection was performed partly with a low-temperature Weissenberg camera, partly with a three-circle goniometer

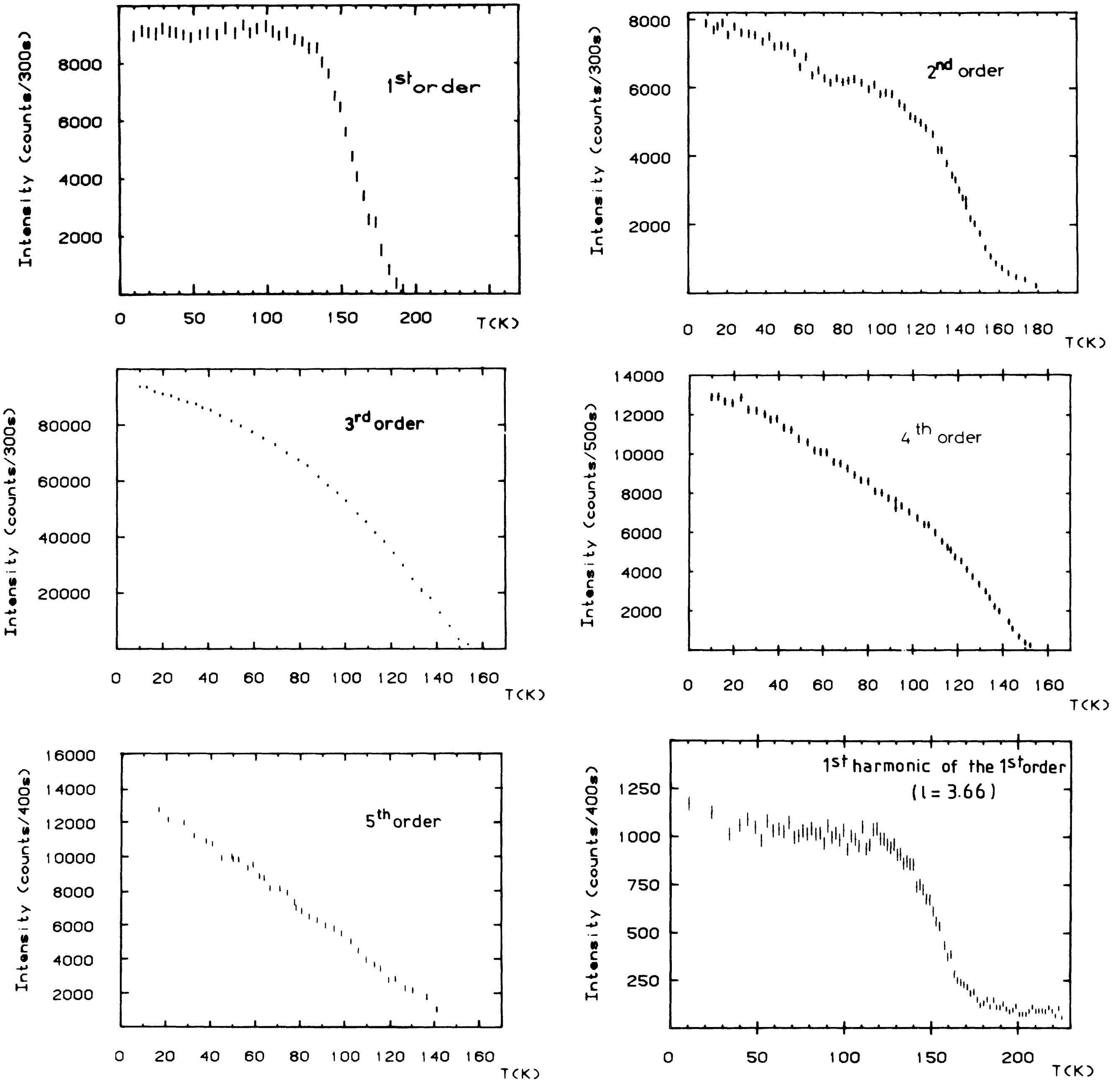

FIG. 13. Temperature dependence of the intensity of iodine Bragg reflections collected on main lines $l=1$ to $l=5$ and on the first harmonic of modulation of main line $l=1$ (at $l=3.66$).

on planes $(h\ k\ l)$ for l ranging from 1 to 7.

The average structure is deduced from the Bragg reflections collected on the main lines and the modulation by the host lattice from the Bragg reflections of the satellites lines.

a. Average structure. Within the accuracy of our measurements the iodine sublattice keeps the tetragonal symmetry. The tetragonal axis is parallel to the c axis of the host lattice $d=9.705$ Å. It is possible to keep the a and b axis of the host lattice to describe the iodine sublattice but the repeat unit becomes $2a\times 2a$, a being the parameter of the host lattice: $a=19.60$ Å. In this unit cell, the extinction conditions are $h'+l=2n+1$ and $k'+l=2m+1$, with n and m integers.

It is more convenient to use a smaller unit cell of parameters $(a\sqrt{2}a,\sqrt{2},d)$ with the basis plane axis parallel to the bisectors of the $\mathbf{a},\mathbf{b}$ axis of the host lattice unit cell. The new extinction conditions are $h''+k''+l=2n+1$. Every unit cell contains eight triiodide chains.

In addition to the phase of each iodine chain, four adjustable parameters were used. The position of the channel labeled 1 on Fig. 17 is described by its coordinates (x,y) in the $\mathbf{a}+\mathbf{b}$ and $\mathbf{a}-\mathbf{b}$ directions, the triiodide molecule is described by the parameter δ already introduced in Sec. IV and an isotropic Debye-Waller factor is introduced.

A reliability factor $R=\sum |I_{\rm obs}-I_{\rm calc}| / \sum I_{\rm obs}=0.05$ was obtained with the relative phase shifts shown on Figs. 17 and 18 and the following adjustable parameter.

(i) Position of the channels $x=6.10$ Å and $y=0$, in perfect agreement with the room-temperature determination.[11,12]

(ii) The distance between two iodine atoms of an I_3^- unit is $\delta\simeq 3.00$ Å. This is the same value as the room-temperature determination (see Sec. IV).

(iii) An isotropic Debye-Weller factor $B=1.4$ Å^2 $(u_{\rm eq}=0.33$ Å$)$.

The space group of the iodine sublattice is $I\bar{4}2d$. The corresponding unit cell with its symmetry elements is represented in Fig. 18. It must be noted that the center of inversion of the inversion tetrad is at $z=d/8$. The phase ordering between the iodine chains shown on Figs. 17 and 18 is not yet understood. In principle, its determination at $T=0$ requires the knowledge of the Coulomb interaction, more or less screened by the DIPSΦ_4 columns, between an iodine chain and its first neighbors. If one considers only

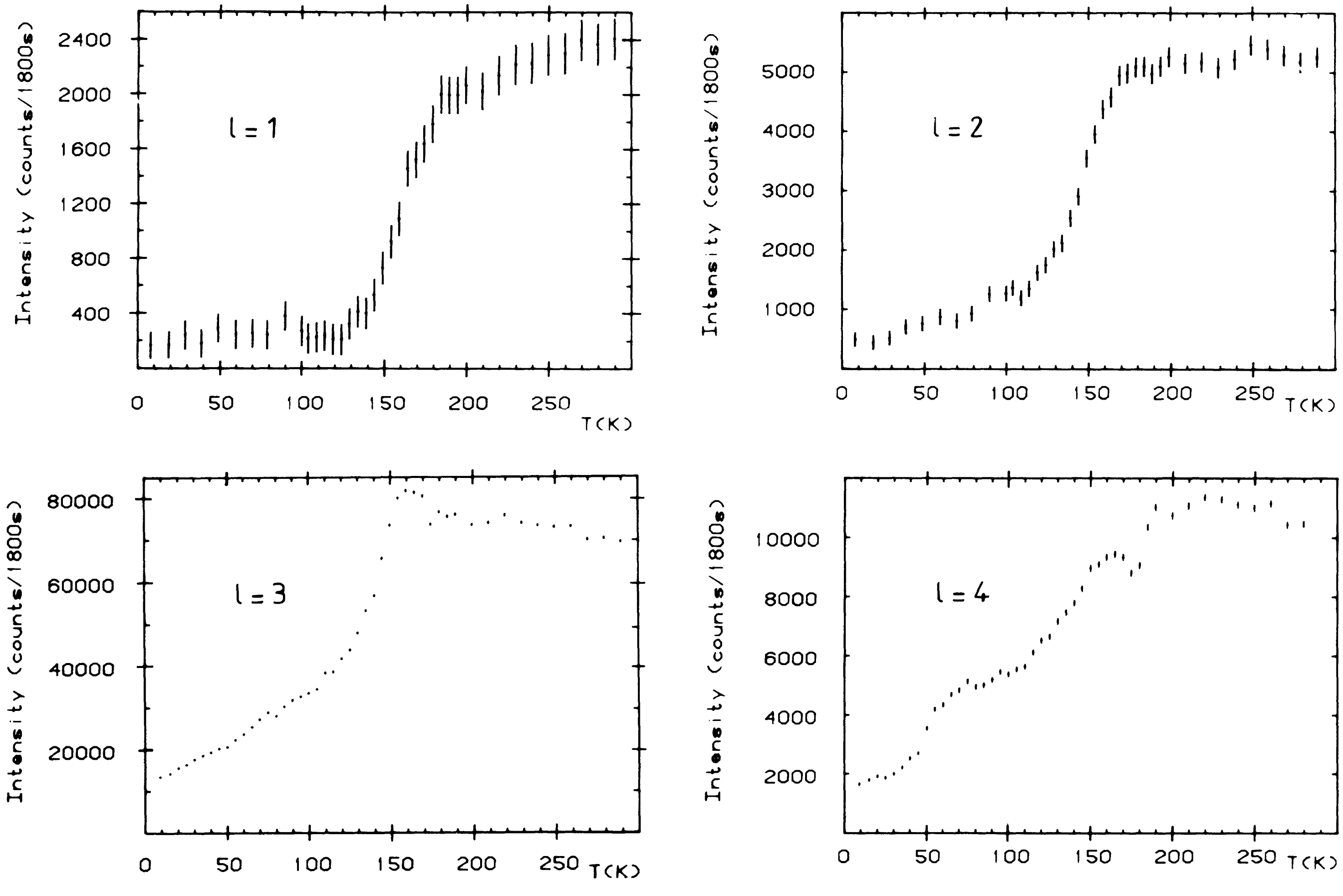

FIG. 14. Temperature dependence of the integrated intensity of the main diffuse lines $l=1$ to $l=4$ taken midway between Bragg reflections.

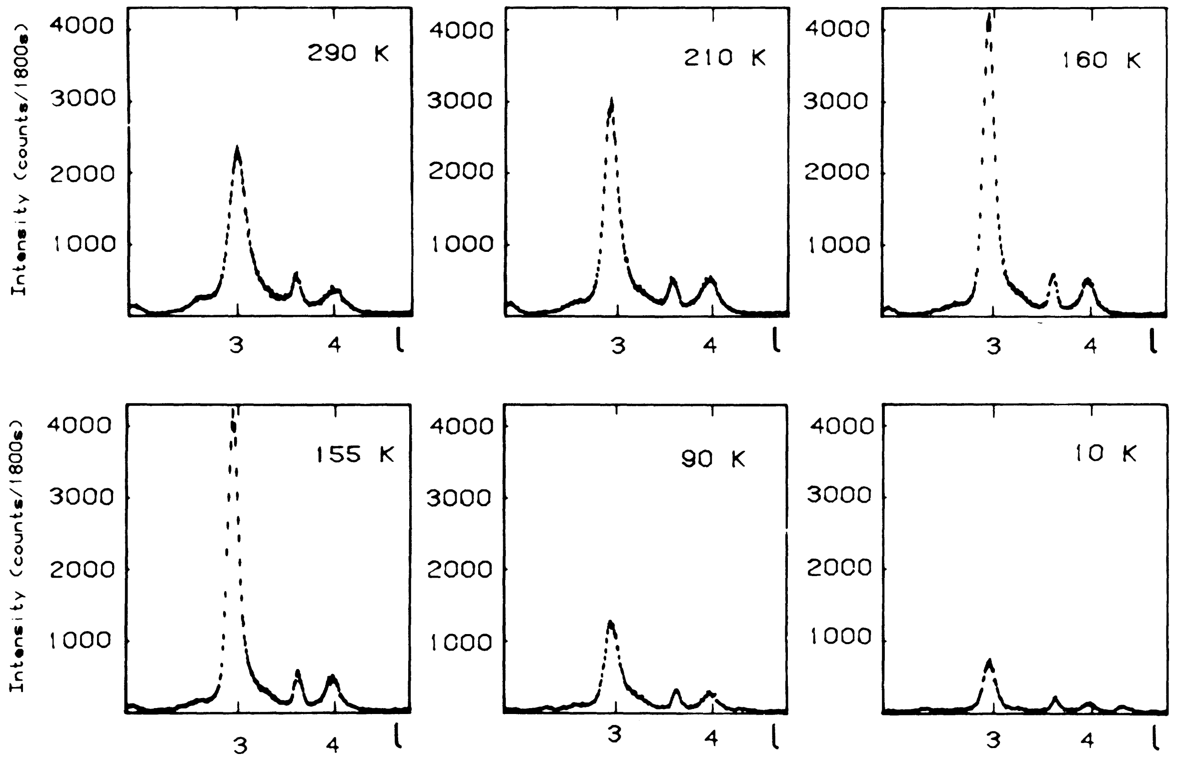

FIG. 15. Position-sensitive detector scans in the c direction of main lines $l=3$, $l=4$ and of the satellite line $l=3.66$ at $T=290$, 210, 160, 155, 90, and 10 K. The scans have been performed midway between Bragg reflections.

the first Fourier component $\rho(1)$ of the ionic density on each chain, one readily sees that for symmetry reasons there is no Coulomb interaction between a chain of phasis 0 or $\frac{1}{2}$ and the chains of phasis $\frac{1}{4}$ and $\frac{3}{4}$. A more complex mechanism including the DIPSΦ_4 columns or the second-order Fourier component $\rho(2)$ is necessary to get an interaction between these chains.

b. Host lattice modulation. 154 Bragg reflections have been collected on the additional lines. They correspond only to indexes for which the molecular structure factor of I_3^- units reinforces strongly the scattered intensity. That is the case of the first harmonic of modulation of main lines 1 (at $l=3.66$) and 4 (at $l=6.66$) and only of the second harmonic of modulation of main lines 1 ($l=6.32$).

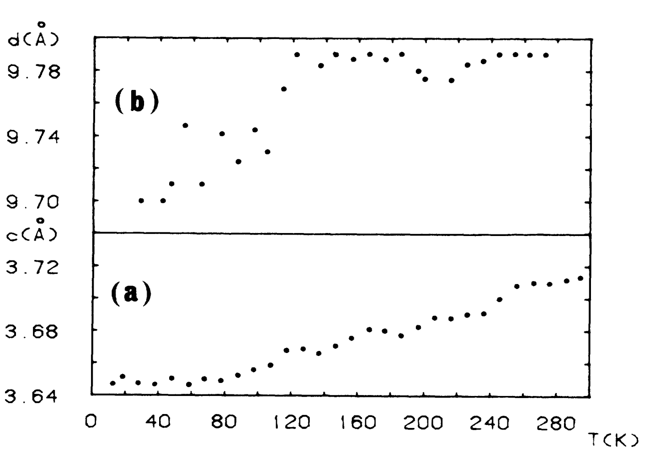

FIG. 16. Temperature dependence of the parameters c (a) and d (b). The precision on the measure of c is about 0.1% and on the measure of d about 0.5%.

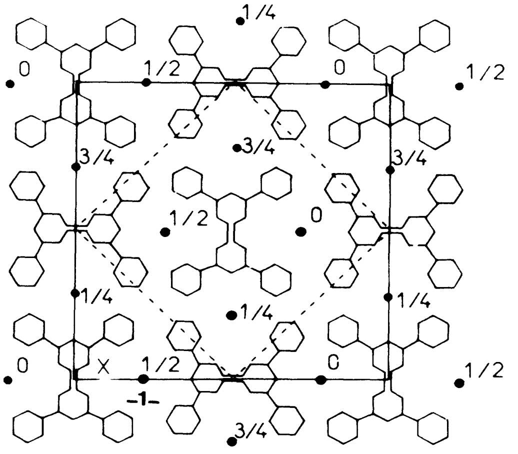

FIG. 17. Low-temperature structure of the iodine sublattice. The numbers give the positions of the triiodide units in the channel direction in fraction of the triiodide chain parameter $d=9.705$ Å at $T=10$ K. The value of the parameter X is 6.10 Å. The interrupted line gives the host lattice unit cell.

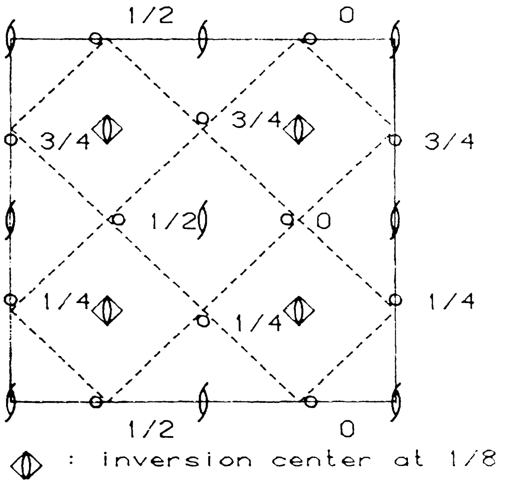

FIG. 18. (001) projection of the iodine sublattice unit cell with its symmetry elements. Note that the inversion center of the inversion tetrad is at $z=\frac{1}{8}d$.

We have found that the planes $(h\,k\,l=3.66)$ and $(h\,k\,l=6.66)$ of satellite reflections are merely the images of the planes $(h\,k\,l=1)$ and $(h\,k\,l=4)$ with only a scale factor. The plane $(h\,k\,l=6.32)$ containing the second-harmonic reflections of the plane $(h\,k\,l=1)$ is also its image. It means that the amplitude of the modulation is the same for all the chains and that the modulation is purely polarized in the channel direction. This result can be easily understood because the external potential exercized by the host lattice is the same for all chains.

As has been noted above, the iodine sublattice is commensurate with the host lattice at low temperature. The unit cell common to both lattices has the parameters $(a\sqrt{2},a\sqrt{2},3d)$ or $(a\sqrt{2},a\sqrt{2},8c)$. It can be easily shown that the corresponding space group is $I\bar{4}2d$. The superstructure intensities can be accounted for by a sinusoidal displacement of the I_3^- units in chain direction of amplitude $\mu=0.23$ Å and wave vector $c^*=2\pi/c=16\pi/3d$. This value is about twice the room temperature value (see Sec. IV). The general phase shift of the iodine sublattice with respect to the organic matrix could not be determined as the DIPSΦ_4 contribution to the superstructure intensities is negligible.

B. Discussion

1. Behavior of the order parameters

We can discuss these results in the framework of the mean-field theory developed by Emery and Axe.[16] If one neglects the modulation exercized by the host lattice, the average particle density below T_c can be written as

$$\langle\rho(z)\rangle=\sum_l\langle\rho(l)\rangle\exp\left[\frac{2i\pi lz}{d}\right].$$

The effective mean-field potential exercized on a chain by its neighbors can be written as $\sum_l v(l)\langle\rho(l)\rangle$, where $v(l)$ is the coupling defined in Sec. V.

As $v(l)$ should rapidly decrease with increasing l (see Sec. V), Emery-Axe theory retains only the first term $v(1)\langle\rho(1)\rangle$. Furthermore, $v(1)$ is supposed to be temperature independent in their theory. $\langle\rho(1)\rangle$ is the primary order parameter found by self-consistency condition.[16] Figure 19 displays the predicted temperature dependence of $|\langle\rho(l)\rangle|^2$ for l ranging from to 1 to 5. Although the theory explains the progressive development of the components $|\langle\rho(l)\rangle|^2$, it predicts a growth much less rapid than what is experimentally observed (Fig. 13). As the distance between iodine atoms in the I_3^- anions does not vary significantly between room temperature and 13 K (see paragraph VI A 3 *a*), this cannot be attributed to an effect of molecular structure factor. Two explanations can be proposed for this. The first one supposes that the contribution of higher-order terms in the mean-field potential is not negligible. In fact, this leads only to minor changes in the temperature dependence unless this contribution is very important.[27] A second explanation is that the coupling coefficient $v(1)$ is temperature dependent. As shown on Fig. 1 the interaction between triiodide chains is a least partially mediated by the host lattice. The coupling $v(1)$ should thus depend upon the electronic state of the DIPSΦ_4 chains. Very crudely, and in relationship with the conductivity measurements performed in Sec. III, a metallic stack should screen the interaction more strongly than a semiconducting stack. Furthermore, this coupling should increase with the increase of the electrical gap [related to Δ_{eff} shown in Fig. 2(b)]. A further hint in the physics of the phase transition comes from the remark that the wave vector of the first Fourier component of the particle density $2\pi/d$ is equal to the $2k_F$ vector of the 1D electronic gas of the DIPSΦ_4 matrix. This fact has been already pointed out in Ref. 9. It makes a link between the iodine ordering process which is the object of Secs. V and VI of this paper and a possible Peierls distortion of the organic lattice which is characterized by the conductivity measurements of Sec. III. With these ingredients one can propose the following mechanism: as

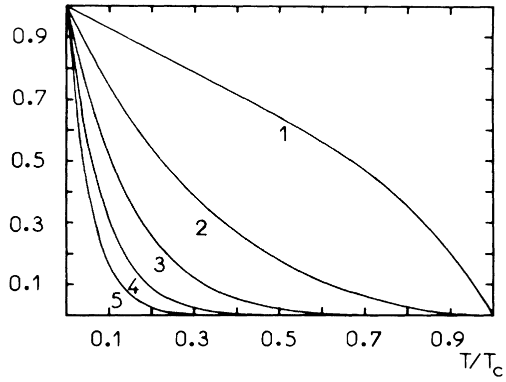

FIG. 19. Temperature dependence of the square of the first five order parameters given by the mean-field theory of Ref. 16.

seen in Sec. V, ordering fluctuations develop significantly on the first main diffuse line below 220 K. Their effect on the DIPSΦ_4 electronic gas is to provide a fluctuating potential at the $2k_F$ wave vector inducing Peierls pretransitional effects. The formation of a pseudogap might be responsible for the decrease of the electrical conductivity below about 220 K [Fig. 2(a)]. At T_c, the apparition of a long-range iodine potential at the wave vector $2k_F$ induces a Peierls transition on the DIPSΦ_4 chains, that is the opening of a gap at $\pm k_F$ in the band structure. As $\langle \rho(1) \rangle$ develops, the potential exercized on the electronic gas increases and thus the gap increases. In counterpart the screening by the DIPSΦ_4 chains of the triiodide interaction is less effective. This leads to an increase of the triiodide interchain interaction. The growth of the order parameters should be thus more rapid than predicted by the Emery-Axe theory. However, Fig. 2(b) shows that Δ_{eff} increases more rapidly below about 150 K. Such an effect might be due to an intrinsic Peierls distortion of the organic stack. Whatever its origin, the rapid increase of Δ_{eff} strengthens the triiodide interchain interactions. This might explain the saturation of $\langle \rho(1) \rangle$ and the faster growth of the other Fourier components of the particle density below this temperature. Numerical calculations are in progress to explain quantitatively these features.[30]

The effect of the commensurability has not been considered. As has been quoted above, it is difficult to find out exactly at which temperature the system becomes commensurate. However the phenomenon of the modulation of the iodine sublattice by the host lattice remains weak and should not play a driving role, because the order of commensurability between the two sublattices ($3d=8c$) is high.

2. *"Liquid fluctuations" below T_c*

The diffuse lines observed below T_c correspond to the scattering by the excitations of the system. No calculation of the dynamical structure factor $S(q,\omega)$ or of the instantaneous one $S\,(q,t=0)$ has been performed below T_c. However, Emery and Axe theory predicts that the excitation spectrum should mainly consist of soliton-antisoliton pairs.[16] In 1D liquids the excitations correspond to quasiphonons damped by the absence of long-range order.[17] This damping accounts for the broadening of the diffuse lines. Below T_c, the various Fourier components of the long-range order develop progressively, but the propagation of the excitations along the channels remains probably damped as evidenced by the presence of still broadened diffuse lines.

In $Hg_{3-\delta}AsF_6$, one-dimensional acoustic quasiphonons have been observed at room temperature.[14(a)] Below the 120-K ordering phase transition, small gaps ($\sim$0.1 meV, i.e., 1.2 K) develop in the Hg-chain phonon dispersion relation.[14(c)] If a similar phenomenon occurs below T_c in DIPS$\Phi_4(I_3)_{0.76}$ with gaps of about the same order of magnitude, the excitation modes are equally populated even at very low temperature, giving rise to the observed x-ray diffuse lines.

VII. CONCLUSION

DIPS$\Phi_4(I_3)_{0.76}$ is a clear example of intercalated compound with an organic matrix delimiting parallel channels filled with triiodide anions. At room temperature, the triiodide chains are nearly decoupled and present the spatial character of a 1D liquid (absence of long-range order). We have shown that a very simple 1D harmonic liquid model accounts well for the observed x-ray diffuse scattering. Furthermore, the position of I_3^- units in channel direction is modulated by the external potential created by the host lattice.

As the temperature is lowered, triiodide chains coupled leading to an ordered phase below $T_c \simeq 182$ K. The development of the long-range order has been followed as a function of temperature and the phase shift between the chains has been determined.

Existing theory accounts for this behavior only qualitatively.[16] A quantitative understanding requires a more general theory including the coupling of the $2k_F$ component of the potential created by the iodine chains with the degrees of freedom of the one-dimensional electronic gas of the organic matrix. In this respect, DIPS$\Phi_4(I_3)_{0.76}$ is a model compound where a detailed study of the coupling of positional degrees of freedom of the anion chains with a Peierls instability of the organic chains could be performed. Previously, the coupling between the electronic degree of freedom of an organic chain and an external potential due to orientational or spin degrees of freedom was observed, respectively, in the tetramethyltetraselenafulvalenium $(TMTSF)_2X$ series,[28] with X a noncentrosymmetric anion and $(\text{Perylene})_2M(mnt)_2$ series[29] with $M=$Pt, Pd on structural and electronic properties and *mnt* signifying 1,2-dicyanoethylene-1,2-dithiol. This coupling led in some of these compounds to a $2k_F$ distortion of the organic stack.

Another class of intercalated iodine chain organic materials contains $TTT_2I_{3+\delta}$, $E_2PI_{1.6}$, and $B_2PI_{1.6}$, where there is one iodine chain per organic chain. In this case, the first Fourier component of the 1D liquid corresponds to the $4k_F$ wave vector of the 1D electronic gas. The coupling between the 1D liquid and the organic host lattice should be thus very different, leading to a different temperature dependence of the order parameters of those systems. As a hint, the conductivity of $TTT_2I_{3+\delta}$ still increases well below the ordering temperature of the iodine sublattice (about 170 K),[14] showing that the electronic properties of the organic stack are not substantially modified by the structural phase transition.

ACKNOWLEDGMENTS

We would like to thank L. Deschamps, S. Megtert, R. Moret, D. Peterman, and C. Weyl for their help in the experimental part. Special thanks are due to C. Noguera for many discussions during the course of this study. Useful discussions with G. Collin, P. Le Guennec, H. J. Schulz, and G. Shirane are also acknowledged.

[1] R. Williams, C. Lowe Ma, and S. Samson, Appl. Phys. Commun. **1**, 223 (1981).

[2] (a) S. Megtert, J. P. Pouget, R. Comès, and R. Fourme, *Quasi One-Dimensional Conductors II*, Vol. 96 of *Lecture Notes in Physics*, edited by S. Barišić, A. Bjeliš, J. R. Cooper, and B. Leontic (Springer-Verlag, Berlin, 1979), p. 196. (b) S. K. Khanna, S. P. S. Yen, R. B. Somoano, P. M. Chaikin, C. Lowe Ma, R. Williams, and S. Samson, Phys. Rev. B **19**, 655 (1979). (c) A. Fihlol, J. Gaultier, C. Hauw, B. Hilti, and C. W. Mayer, Acta Crystallogr. B **38**, 2577 (1982).

[3] H. Endres, J. P. Pouget, and R. Comès, J. Phys. Chem. Solids **43**, 739 (1982).

[4] V. F. Kaminskii, M. L. Khidekel, R. B. Lubovskii, I. F. Shegolev, R. P. Shibaeva, E. B. Yagubskii, A. V. Zvarykina, and T. I. Zverena, Phys. Status Solidi **44A**, 77 (1977).

[5] C. Lowe Ma, R. Williams, and S. Samson, J. Chem. Phys. **74**, 1966 (1981).

[6] E. Rosshirt, F. Frey, H. Boysen, and H. Jagodzinski, Acta Crystallogr. B **41**, 66 (1985).

[7] H. Endres, R. Harms, H. J. Keller, W. Moroni, D. Nöthe, M. H. Vartanian, and Z. G. Soos, J. Phys. Chem. Solids **40**, 591 (1979).

[8] (a) H. Strzelecka, C. Weyl, and J. Rivory, *Quasi One-Dimensional Conductors II*, Vol. 96 of *Lecture Notes in Physics*, edited by S. Barišić, A. Bjeliš, J. R. Cooper, and B. Leontic (Springer-Verlag, Berlin, 1979). (b) H. Strzelecka and J. Rivory, Mater. Res. Bull. **15**, 899 (1980). (c) C. Fabre, R. Fugnitto, and H. Strzelecka, C. R. Acad. Sci. Paris, **C282**, 175 (1976).

[9] L. C. Isett, G. A. Reynolds, E. M. Schneider, and J. H. Perlstein, Solid State Commun. **30**, 1 (1979).

[10] J. Amiell, P. Delhaes, S. Flandrois, and H. Strzelecka, Solid State Commun. **39**, 55 (1981).

[11] H. R. Luss and D. L. Smith, Acta Crystallogr. B **36**, 1580 (1980).

[12] D. Chasseau, J. Gaultier, C. Hauw, S. Lefrant, R. Rivory, E. Rzepka, and H. Strzelecka, Solid State Commun. **34**, 873 (1980).

[13] P. A. Albouy, J. P. Pouget, and H. Strzelecka, J. Phys. (Paris) **44**, C3 1339 (1983).

[14] (a) J. M. Hastings, J. P. Pouget, G. Shirane, A. J. Heeger, N. D. Miro, and A. G. McDiarmid, Phys. Rev. Lett. **39**, 1484 (1977). (b) J. P. Pouget, G. Shirane, J. M. Hastings, A. J. Heeger, N. D. Miro, and A. G. McDiarmid, Phys. Rev. B **18**, 3645 (1978). (c) I. U. Heilman, J. M. Hastings, G. Shirane, A. J. Heeger, and A. G. McDiarmid, Solid State Commun. **29**, 469 (1979). (d) I. U. Heilman, J. D. Axe, J. M. Hastings, G. Shirane, A. J. Heeger, and A. G. McDiarmid, Phys. Rev. B **20**, 751 (1979). (e) R. Spal, C. E. Chen, T. Egami, and A. J. Heeger, Phys. Rev. B **21**, 3110 (1980). (f) J. D. Axe, D. B. McWhan, and P. J. Nigrey, Phys. Rev. B **27**, 3845 (1983).

[15] (a) I. D. Brown, B. D. Cutforth, C. G. Davies, R. J. Gillespie, P. R. Ireland, and J. E. Vekris, Can. J. Chem. **52**, 791 (1974). (b) A. J. Schultz, J. M. Williams, N. D. Miro, A. G. McDiarmid, and A. J. Heeger, Inorg. Chem. **17**, 646 (1978).

[16] (a) J. D. Axe, in *Solitons and Condensed Matter Physics*, Vol. 8 of *Solid State Sciences* (Springer-Verlag, Berlin, 1978). (b) V. J. Emery and J. D. Axe, Phys. Rev. Lett. **40**, 1507 (1978).

[17] T. Yoshida, K. Shobu, and H. Mori, Prog. Theor. Physics **66**, 759 (1981).

[18] M. Lemonnier, D. Petermann, D. Lefur, and S. Megtert, Centre National de la Recherche Scientifique (C.N.R.S.) Patent No. 8203344 (France).

[19] B. K. Vainshtein, in *Diffraction of X Rays by Chains Molecules*, Amsterdam, London, (Elsevier, New York, 1966).

[20] P. A. Albouy, P. Keller, and J. P. Pouget, J. Am. Chem. Soc. **104**, 6556 (1981).

[21] M. Kertész and F. Vonderviszt, J. Am. Chem. Soc. **104**, 5889 (1982).

[22] A. Bunde, Z. Phys. B **44**, 225 (1981).

[23] T. Geisel, Solid State Commun. **32**, 739 (1979).

[24] See for instance, J. P. Pouget, in *Solid State Phase Transformations in Metals and Alloys* (Editions de Physique, Orsay, 1978), p. 523.

[25] J. I. Langford, J. Appl. Crystallogr. **11**, 10 (1978).

[26] P. A. Albouy and J. P. Pouget (unpublished).

[27] P. Le Guennec and C. Noguera (unpublished).

[28] See for instance R. Moret, J. P. Pouget, R. Comès, and K. Bechgaard, J. Phys. (Paris) Colloq. **44**, C3-957 (1983).

[29] R. T. Henriques, L. Alcacer, J. P. Pouget, and D. Jérome, J. Phys. C **17**, 5197 (1984).

[30] P. A. Albouy, P. Le Guennec, J. P. Pouget, and C. Noguera, (ICSM) Kyoto, 1986 [Synth. Met. (to be published)].

[31] The real charge distribution on a linear chain of triiodide anions has not yet been calculated. It should be intermediate between that of formula (17) and that of a free anion [$0.5e^-$ on each outer iodine atom: W. Gabes and A. M. Nijman-Meester, Inorg. Chem. **12**, 589 (1973)].

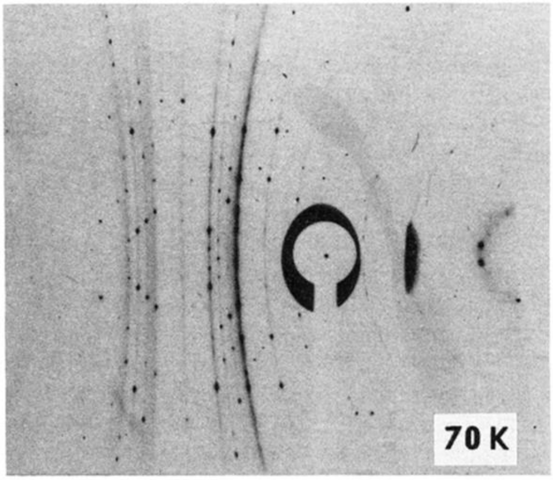

FIG. 12. X-ray pattern obtained in the same conditions as in Fig. 7 but with $T=70$ K. Bragg reflections are visible on all the diffuse lines.

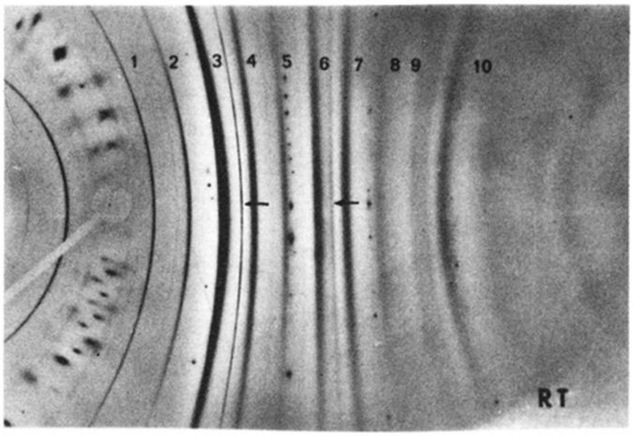

FIG. 3. Fixed-film fixed-crystal x-ray pattern of the DIPS$\Phi_4(I_3)_{0.76}$ single crystal taken at station D16 of LURE at room temperature ($\lambda = 1.06$ Å). The *c* axis is horizontal, *l* indices are for main lines, arrows for additional lines.

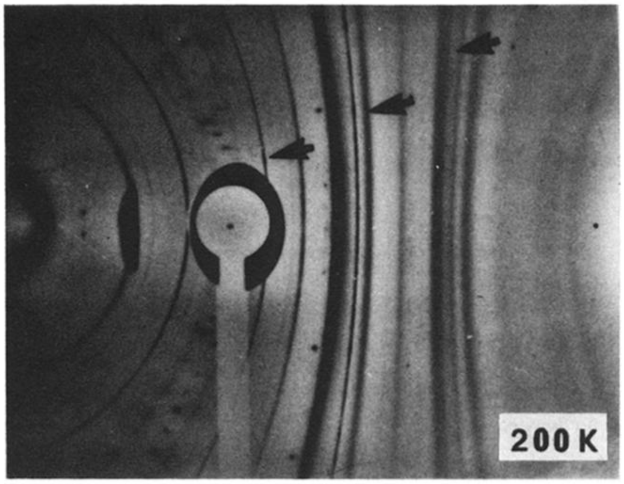

FIG. 7. Fixed-film crystal x-ray pattern of a DIPS$\Phi_4(I_3)_{0.76}$ single crystal taken at station D16 of LURE at 200 K ($\lambda = 1.58$ Å). The *c* axis is horizontal. Arrows point to intensity reinforcements on the first main line and its first harmonic of modulation. Right-hand arrow points to the second harmonic of modulation of the first main line.

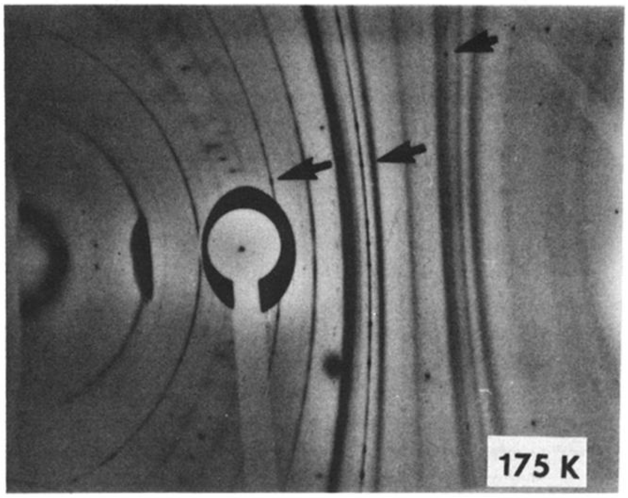

FIG. 8. X-ray pattern obtained in the same conditions as in Fig. 7 but with $T = 175$ K. Bragg reflections are visible on the first main line and its satellites of modulation.